ORGANOMETALLICS

Article

pubs.acs.org/Organometallics

Unusual C−C Bond Cleavage in the Formation of Amine-Bis(phenoxy) Group 4 Benzyl Complexes: Mechanism of Formation and Application to Stereospecific Polymerization

Ravikumar R. Gowda,[†] Lucia Caporaso,*[,‡] Luigi Cavallo,[§] and Eugene Y.-X. Chen*[,†]

[†]Department of Chemistry, Colorado State University, Fort Collins, Colorado 80523-1872, United States

[‡]Dipartimento di Chimica e Biologia, Università di Salerno, Via Giovanni Paolo II, I-84084, Fisciano, Italy

[§]Physical Sciences and Engineering Division, King Abdullah University of Science and Technology (KAUST), Kaust Catalysis Center, Thuwal 23955-6900, Saudi Arabia

Supporting Information

ABSTRACT: Group 4 tetrabenzyl compounds MBn_4 (M = Zr, Ti), upon protonolysis with an equimolar amount of the tetradentate amine-tris(phenol) ligand N-[(2,4-^{t}Bu$_2$C$_6$H$_2$(CH$_2$)OH]$_3$ in toluene from −30 to 25 °C, unexpectedly lead to amine-bis(phenoxy) dibenzyl complexes, BnCH$_2$N[(2,4-^{t}Bu$_2$C$_6$H$_2$(CH$_2$)O]$_2$MBn$_2$ (M = Zr (**1**), Ti (**2**)) in 80% (**1**) and 75% (**2**) yields. This reaction involves an apparent cleavage of the >NCH$_2$−ArOH bond (loss of the phenol in the ligand) and formation of the >NCH$_2$−CH$_2$Bn bond (gain of the benzyl group in the ligand). Structural characterization of **1** by X-ray diffraction analysis confirms that the complex formed is a bis(benzyl) complex of Zr coordinated by a newly derived tridentate amine-bis(phenoxy) ligand arranged in a *mer* configuration in the solid state. The abstractive activation of **1** and **2** with B(C$_6$F$_5$)$_3$·THF in CD$_2$Cl$_2$ at room temperature generates the corresponding benzyl cations {BnCH$_2$N[(2,4-^{t}Bu$_2$C$_6$H$_2$(CH$_2$)O]$_2$MBn(THF)}$^+$[BnB(C$_6$F$_5$)$_3$]$^-$ (M = Zr (**3**), Ti, (**4**)). These cationic complexes, along with their analogues derived from (imino)phenoxy tri- and dibenzyl complexes, [(2,6-^{i}Pr$_2$C$_6$H$_3$)N=C(3,5-^{t}Bu$_2$C$_6$H$_2$)O]ZrBn$_3$ (**5**) and [2,4-Br$_2$C$_6$H$_2$(O)(6-CH$_2$(NC$_5$H$_9$))CH$_2$N=CH(2-adamantyl-4-MeC$_6$H$_2$O)]ZrBn$_2$ (**6**), have been found to effectively polymerize the biomass-derived renewable *β*-methyl-*α*-methylene-*γ*-butyrolactone ($_\beta$MMBL) at room temperature into the highly stereoregular polymer P$_\beta$MMBL with an isotacticity up to 99% *mm*. A combined experimental and DFT study has yielded a mechanistic pathway for the observed unusual C−C bond cleavage in the present protonolysis reaction between $ZrBn_4$ and N[(2,4-^{t}Bu$_2$C$_6$H$_2$(CH$_2$)OH]$_3$ for the formation of complex **1**, which involves the benzyl radical and the Zr(III) species, resulting from thermal and photochemical decomposition of $ZrBn_4$, followed by a series of reaction sequences consisting of protonolysis, tautomerization, H-transfer, oxidation, elimination, and radical coupling.

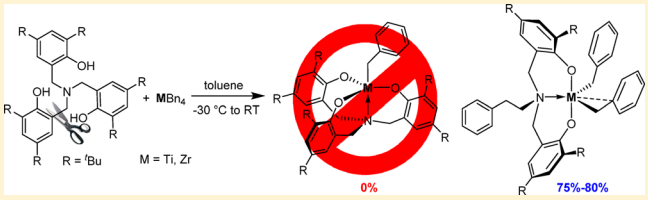

INTRODUCTION

Efforts in exploring naturally occurring or biomass-derived renewable resources to replace dwindling petroleum-based raw materials in large commodity markets, such as chemicals, materials, and fuels, have been expedited in recent years.[1−6] In the context of developing sustainable polymeric materials based on renewable monomers, a large number of compounds comprising an *α*-methylene-*γ*-butyrolactone moiety, which have been found and extracted from multifarious plants,[7] are of potential interest. Tulipaline A, or *α*-methylene-*γ*-butyrolactone (MBL), found naturally in tulips or produced chemically from biomass feedstocks, is the simplest and the most explored member of the naturally occurring sesquiterpene lactone family.[8] Poly(*α*-methylene-*γ*-butyrolactone) (PMBL) exhibits attractive physical properties, such as a high glass-transition temperature (T_g) of 195 °C,[9] good durability, and a high refractive index of 1.540.[10] The copolymers and blends composed of MBL units render promising optical properties as well as resistance to solvent, weathering, heat, and scratching.[11] Two other monomers well applied in this facet of study are *γ*-methyl and *β*-methyl derivatives of MBL, *γ*-methyl-*α*-methylene-*γ*-butyrolactone ($_\gamma$MMBL) and *β*-methyl-*α*-methylene-*γ*-butyrolactone ($_\beta$MMBL). A two-step process from the biomass-derived levulinic acid was developed in the synthesis of $_\gamma$MMBL.[12,13] $_\beta$MMBL was traditionally prepared by a multistep process using petrochemicals,[14−16] but a "sustainable" route from the biomass-derived itaconic acid has recently been developed.[17] Many polymerization methods have been utilized in the polymerization of MBL into low- to high-molecular-weight polymers, through radical,[9,18−23] anionic,[9] group-transfer,[24] and coordination[25] polymerization processes. $_\gamma$MMBL has also been polymerized by free-radical emulsion polymerization[10,26] as well as radical, anionic, and group-transfer polymerization methods.[27] A number of highly active catalyst systems have recently been developed for living and/or

Received: June 20, 2014
Published: July 31, 2014

 © 2014 American Chemical Society

high-speed polymerization of $_{\gamma}$MMBL.[28−34] Similarly, radical polymerization of $_{\beta}$MMBL led to formation of the corresponding atactic polymer,[14] but utilizing the protocol developed for the metal-catalyzed coordination polymerization of polar vinyl monomers,[35] $_{\beta}$MMBL has been converted into highly isotactic or even stereodefect-free polymer P$_{\beta}$MMBL.[15,16,36]

Group 4 nonmetallocene complexes, upon appropriate activation, have been extensively utilized as catalysts for α-olefin polymerization.[37−43] Notable examples of such catalyst systems include 2,2′-ethylenebis[*N*,*N*′-(triisopropylsilyl)-anilinido]zirconium complexes (for living polymerization),[44] an amine-bis(phenolate)titanium benzyl complex (for block copolymerization),[45] group 4 complexes supported by [ONNO]-type bis(*o*-aminophenolato) ligands,[46] bis-(pentafluorophenylamido)zirconium benzyl complexes,[47] sterically hindered chelating phenoxy titanium and zirconium complexes[48] (for living polymerization of 1-hexene),[49] a C_2-symmetric amine-bis(phenolate)zirconium benzyl complex (for isospecific living polymerization of 1-hexene),[50] highly active [ONXO]-type zirconium and hafnium amine-bisphenolate (X = N, O, S) dibenzyl complexes,[51] amine-bis(phenolate) zirconium dibenzyl complexes,[52] titanium, zirconium, and hafnium complexes of an amine-bis(phenolate) ligand containing a THF as well as furan side arm donors,[53] and group 4 complexes of diamine-bis(phenolates).[54] In 2005, Kol and coworkers reported zirconium dibenzyl complexes of chiral salan ligands for isospecific polymerization of 1-hexene and 4-methyl-1-pentene together with cyclopolymerization of 1,5-hexadiene,[55] group 4 dibenzyl complexes of robust salophan ligands for 1-hexene polymerization,[56] C_1-symmetric [ONNO′]-type salan zirconium complexes for 1-hexene polymerization,[57] and salan zirconium complexes for isospecific polymerization of vinylcyclohexane.[58] More recently, Kol et al. employed titanium dibenzyl complexes incorporating salalen (i.e., half-salan/half-salen) ligands for the synthesis of highly isotactic polypropylene.[59] Waymouth et al. recently reported group 4 bis-(phenolate)ether dibenzyl complexes for stereospecific propylene polymerization.[60]

Recently, we extended our interest to the coordination polymerization of renewable polar vinyl monomers such as MBL and $_{\gamma}$MMBL to include group 4 achiral (imino)phenoxy-tribenzyl and chiral amino(imino)bis(phenoxy) dibenzyl complexes.[61] The current work was originally intended to synthesize tripodal amine-tris(phenoxy) group 4 monobenzyl complexes through seemingly straightforward protonolysis of group 4 tetrabenzyl complexes MBn_4 (M = Zr, Ti) with the tetradentate amine-tris(phenol) ligand $N[(2,4\text{-}^tBu_2C_6H_2(CH_2)\text{-}OH]_3$ and subsequently investigate their catalytic properties in the coordination polymerization of renewable methylene butyrolactones, particularly $_{\beta}$MMBL, as its coordination polymerization by a non-metallocene catalyst has not been reported prior to this work. However, through the course of this study, we discovered an unusual C−C bond cleavage in the proposed protonolysis reaction, producing the unexpected amine-bis(phenoxy) dibenzyl complexes in good isolated yields (75−80%) with concurrent liberation of the coproducts 2,4-di-*tert*-butylphenol and toluene. Accordingly, the current study has focused on the synthesis, characterization, and activation of such dibenzyl complexes. A combined experimental and DFT study has yielded a mechanistic pathway toward their formation involving the benzyl radical and the Zr(III) species. Furthermore, the generated cationic species have been found to effectively polymerize $_{\beta}$MMBL at room temperature into the highly stereoregular polymer P$_{\beta}$MMBL.

EXPERIMENTAL SECTION

Materials, Reagents, and Methods. All syntheses and manipulations of air- and moisture-sensitive reagents and materials were carried out in flamed Schlenk-type glassware on a dual-manifold Schlenk line, on a high-vacuum line, or in an inert-gas-filled (Ar or N_2) glovebox. NMR-scale reactions were conducted in Teflon-valve-sealed J. Young type NMR tubes. HPLC-grade organic solvents were first sparged extensively with N_2 during filling of 20 L solvent reservoirs and then dried by passage through activated alumina (for Et_2O, THF, and CH_2Cl_2) followed by passage through Q-5 supported copper catalyst (for toluene and hexanes) stainless steel columns. Benzene-d_6 and toluene-d_8 were dried over sodium/potassium alloy and vacuum-distilled or filtered, whereas CD_2Cl_2 and $CDCl_3$ were dried over activated Davison 4 Å molecular sieves. NMR spectra were recorded on a Varian Inova 300 (300 MHz, ^{1}H; 75 MHz, ^{13}C; 282 MHz, ^{19}F), 400, or 500 MHz spectrometer. Chemical shifts for ^{1}H and ^{13}C spectra were referenced to internal solvent resonances and are reported as parts per million relative to $SiMe_4$, whereas ^{19}F NMR spectra were referenced to external $CFCl_3$. Elemental analyses were performed by Robertson Microlit Laboratories, Madison, NJ.

2,4-Di-*tert*-butylphenol, hexamethylenetetramine, triethylamine, 3,5-dibromosalicylaldehyde, paraformaldehyde, and zirconium(IV) chloride were purchased from Alfa Aesar Chemical Co. Benzylmagnesium chloride, 2-(aminomethyl)piperidine, 3,5-di-*tert*-butyl-2-hydroxybenzaldehyde, and titanium(IV) chloride were purchased from Sigma-Aldrich Chemical Co. and used as received. Formaldehyde (36−38% aqueous solution) was purchased from Mallinckrodt Chemicals. Methyl methacrylate (MMA) was purchased from Sigma-Aldrich Chemical Co., and α-methylene-γ-butyrolactone (MBL) and γ-methyl-α-methylene-γ-butyrolactone ($_{\gamma}$MMBL) were purchased from TCI America, while β-methyl-α-methylene-γ-butyrolactone ($_{\beta}$MMBL) was prepared according to literature procedures.[17] These monomers were first degassed and dried over CaH_2 overnight, followed by vacuum distillation; MMA was further purified by titration with neat tri-*n*-octylaluminum to a yellow end point and distillation under reduced pressure. The purified monomers were stored in brown bottles inside a glovebox freezer at −30 °C. Butylated hydroxytoluene (BHT-H, 2,6-di-*tert*-butyl-4-methylphenol) was purchased from Alfa Aesar Chemical Co. BHT-H was recrystallized from hexanes prior to use. Tris-(pentafluorophenyl)borane, $B(C_6F_5)_3$, was obtained as research gift from Boulder Scientific Co. and was further purified by sublimation. $B(C_6F_5)_3$·THF was prepared by addition of THF to a toluene solution of the borane at ambient temperature, followed by removal of the volatiles and drying under vacuum.

Tetrabenzyltitanium and tetrabenzylzirconium were prepared according to published procedures[62a] and used shortly thereafter. The ligands 6,6′,6″-nitrilotris(methylene)tris(2,4-di-*tert*-butylphenol),[63] 3-adamantyl-2-hydroxy-5-methylbenzaldehyde,[64] 2-(bromomethyl)-4,6-dibromophenol,[59] and 2,4-di-*tert*-butyl-6-((2,6-diisopropylphenylimino)methyl)phenol ($(2,6\text{-}^iPr_2C_6H_3)N{=}C\text{-}(3,5\text{-}^tBu_2C_6H_2)OH$)[65] and $[(2,6\text{-}^iPr_2C_6H_3)N{=}C(3,5\text{-}^tBu_2C_6H_2)O]\text{-}ZrBn_3$ (**5**),[61] $[(2,6\text{-}^iPr_2C_6H_3)N{=}C(3,5\text{-}^tBu_2C_6H_2)O]TiBn_3$ (**6**),[61] and $[2,4\text{-}Br_2C_6H_2(O)(6\text{-}CH_2(NC_5H_9))CH_2N{=}CH(2\text{-adamantyl-}4\text{-}MeC_6H_2O)]ZrBn_2$ (**7**)[61] were synthesized according to literature procedures.

Synthesis and Structural Characterization of $BnCH_2N[(2,4\text{-}^tBu_2C_6H_2(CH_2)O]_2ZrBn_2$ (1). The following reaction was performed in a glass reactor wrapped with Al foil to minimize exposure to light. A solution of $N[(2,4\text{-}^tBu_2C_6H_2(CH_2)OH]_3$ (0.50 g, 0.74 mmol) in toluene (10 mL) and a solution of $ZrBn_4$ (0.34 g, 0.74 mmol) in toluene (10 mL) were precooled at −30 °C inside the glovebox for 6 h. After the two solutions were mixed, a pale orange color appeared instantly and then disappeared slowly to form a colorless solution. Stirring continued for 24 h at room temperature, after which the solvent was removed under reduced pressure to afford a colorless powder. This powder was further purified by crystallization

dx.doi.org/10.1021/om500661y | *Organometallics* 2014, 33, 4118−4130

from toluene at −30 °C to afford **1** as a colorless solid (0.49 g, 80%). Anal. Calcd for $C_{52}H_{67}NO_2Zr{\cdot}C_7H_8$: C, 76.90; H, 8.20; N, 1.52. Found: C, 77.18; H, 8.78; N, 2.11.

^{1}H NMR (C_6D_6, 23 °C): δ 7.64−7.61 (m, 5H, Ar-*H*), 7.16−6.65 (m, 17H, Ar-*H*, C_7H_8), 6.48−6.46 (m, 2H, Ar-*H*), 3.40 (d, J = 12 Hz, 2H, Ar-CH_2), 3.07 (d, J = 12 Hz, 2H, Ar-CH_2), 2.82 (s, 2H, CH_2-N), 2.45−2.29 (m, 4H, Ar-CH_2-Zr), 2.11 (s, C_7H_8), 2.02 (s, 2H, NCH$_2$CH_2Ph), 1.75 (s, 18H, Ar-C(CH_3)$_3$), 1.43 (s, 18H, Ar-C(CH_3)$_3$). ^{13}C NMR (C_6D_6, 23 °C): δ 157.9 (*Ar*-O-Zr), 147.2 (*Ar*-CH$_2$-Zr), 141.4 (*Ar*-C(CH$_3$)$_3$), 137.9 (C_7H_8), 136.9 (*Ar*-C(CH$_3$)$_3$), 136.4 (Ar-*C*), 130.5 (Ar-*C*), 129.3 (C_7H_8), 129.0 (Ar-*C*), 128.9 (Ar-*C*), 128.7 (Ar-*C*), 128.6 (Ar-*C*), 128.5 (C_7H_8), 126.7 (Ar-*C*), 125.7 (C_7H_8), 125.1 (Ar-*C*), 124.9 (Ar-*C*), 124.7 (Ar-*C*), 124.2 (Ar-*C*), 122.2 (Ar-*C*), 60.4 ($^1J_{C-H}$ = 128.8 Hz, η^1, Ar-CH$_2$-Zr), 60.0 ($^1J_{C-H}$ = 137.7 Hz, η^2, Ar-CH$_2$-Zr), 59.0 (−CH$_2$N), 45.7 (−CH$_2$N), 35.5 (Ar-C(CH$_3$)$_3$), 34.5 (Ar-C(CH$_3$)$_3$), 32.0 (Ar-C(CH$_3$)$_3$), 30.6 (Ar-C(CH$_3$)$_3$), 27.2 (Ar-CH$_2$CH$_2$N), 21.4 (C_7H_8).

The molecular structure of **1** has been confirmed by single-crystal X-ray diffraction analysis. A 20 mL glass vial was charged with 10 mg (0.012 mmol) of **1** and 3 mL of toluene. The solution was carefully layered with 4 mL of hexanes. The vial was cooled to −30 °C and stored inside the glovebox freezer for 7 days to afford colorless single crystals of **1**. After the solvent was decanted, the crystals were quickly coated with a layer of Paratone-N oil (Exxon, dried and degassed at 140 °C/10^{-6} Torr for 16 h) in the glovebox. A crystal was then mounted on a thin glass fiber under a cold stream of dinitrogen gas. Single-crystal X-ray diffraction data were acquired on a Bruker Kappa APEX II CCD diffractometer with Mo Kα radiation (λ = 0.71073 Å) and a graphite monochromator. Initial lattice parameters were obtained from a least-squares analysis of more than 100 reflections; these parameters were later refined against all data. The crystal did not show any significant decay during data collection. Data were integrated and corrected for Lorentz and polarization effects using Bruker APEX2 software, and semiempirical absorption corrections were applied using SCALE.[66a] Space group assignments were based on systematic absences, E statistics, and successful refinement of the structure. The structure was solved by the Patterson method and refined with the aid of successive Fourier difference maps against all data using the SHELXTL 6.14 software package.[66b] Thermal parameters for all non-hydrogen atoms were refined anisotropically, while all hydrogen atoms were assigned to ideal positions and refined using a riding model with an isotropic thermal parameter 1.2 times that of the attached carbon atom (1.5 times for methyl hydrogens). Selected bond distances and angles for compound **1** are collected in the caption of Figure 2. All other metric parameters can be found in the cif file included with the Supporting Information. In the structure the disordered solvent molecule had been found in Fourier difference maps to be disordered over multiple sites. After numerous attempts to model the disorder failed to improve agreement factors, SQUEEZE[66c] was implemented to remove the electron density for the disordered solvent. Selected crystallographic data for **1**: $C_{59}H_{75}NO_2Zr$, triclinic, space group $P\bar{1}$, a = 11.9094(12) Å, b = 16.5817(16) Å, c = 16.6031(16) Å, α = 108.638(4)°, β = 107.622(4)°, γ = 94.550(4)°, V = 2904.2(5) Å^3, Z = 2, D_{calcd} = 1.054 Mg/m^3, GOF = 1.077, R1 = 0.0567 [$I > 2\sigma(I)$], wR2 = 0.1504. CCDC-999630 contains the supplementary crystallographic data. These data can be obtained free of charge from The Cambridge Crystallographic Data Centre via www.ccdc.cam.ac.uk/data_request/cif.

Synthesis of BnCH$_2$N[(2,4-^{t}Bu$_2$C$_6$H$_2$(CH$_2$)O]$_2$TiBn$_2$ (2). The following reaction was performed in a glass reactor wrapped with Al foil to minimize exposure to light. A solution of N-[(2,4-^{t}Bu$_2$C$_6$H$_2$(CH$_2$)OH]$_3$ (0.50 g, 0.74 mmol) in toluene (10 mL) and a solution of TiBn$_4$ (0.31 g, 0.74 mmol) in toluene (10 mL) were precooled at −30 °C inside the glovebox for 6 h. After the solutions were mixed, the red color appeared instantly. Stirring was continued for 24 h at room temperature, after which the solvent was removed under reduced pressure to afford a yellowish brown residue. This residue was further purified by crystallization from toluene layered with hexanes at −30 °C to afford **2** as a yellowish orange solid (0.44 g, 75%). Anal. Calcd for $C_{52}H_{67}NO_2Ti$: C, 79.46; H, 8.59; N, 1.78. Found: C, 79.09; H, 8.45; N, 1.74.

^{1}H NMR (C_6D_6, 23 °C): δ 7.73 (s, 2H, Ar-*H*), 7.25 (d, J = 7.4 Hz, 3H, Ar-*H*), 7.13−7.01 (m, 7H, Ar-*H*, C_7H_8), 6.89−6.83 (m, 4H, Ar-*H*), 6.74 (t, J = 7.5 Hz, 2H, Ar-*H*), 6.62−6.58 (m, 1H, Ar-*H*), 6.43−6.41 (m, 2H, Ar-*H*), 6.33 (t, J = 7.7 Hz, 2H, Ar-*H*), 5.92 (t, J = 7.3 Hz, 1H, Ar-*H*), 3.79 (s, 2H, Ar-CH_2), 3.63 (s, 2H, Ar-CH_2), 2.90−2.74 (m, 6H, Ar-CH_2-Ti, −CH_2N), 2.12 (s, C_7H_8), 2.07 (s, 20H, Ar-C(CH_3)$_3$, −CH_2N), 1.43 (s, 18H, Ar-C(CH_3)$_3$). ^{13}C NMR (C_6D_6, 23 °C): δ 160.1 (*Ar*-O-Ti), 143.6 (*Ar*-CH$_2$-Ti), 143.4 (*Ar*-C(CH$_3$)$_3$), 141.8 (*Ar*-C(CH$_3$)$_3$), 137.6 (C_7H_8), 135.6 (Ar-*C*), 130.1 (Ar-*C*), 129.3 (C_7H_8), 129.0 (Ar-*C*), 128.5 (C_7H_8), 128.4 (Ar-*C*), 128.3 (Ar-*C*), 127.7 (Ar-*C*), 126.3 (Ar-*C*), 125.7 (C_7H_8), 124.8 (Ar-*C*), 124.8 (Ar-*C*), 124.5 (Ar-*C*), 123.4 (Ar-*C*), 123.0 (Ar-*C*), 85.8 ($^1J_{C-H}$ = 134.5 Hz, η^2, Ar-CH$_2$-Ti), 84.1 ($^1J_{C-H}$ = 130.9 Hz, η^1, Ar-CH$_2$-Ti), 59.4 (−CH$_2$N), 46.4 (−CH$_2$N), 35.9 (Ar-C(CH$_3$)$_3$), 34.5 (Ar-C(CH$_3$)$_3$), 32.0 (Ar-C(CH$_3$)$_3$), 31.9 (Ar-C(CH$_3$)$_3$), 26.5 (Ar-CH$_2$CH$_2$N), 21.5 (C_7H_8).

In Situ Generation of {BnCH$_2$N[(2,4-^{t}Bu$_2$C$_6$H$_2$(CH$_2$)O]$_2$ZrBn(THF)}$^+$[BnB(C$_6$F$_5$)$_3$]$^-$ (3). Cationic species **3** was generated by in situ mixing of **1** and B(C_6F_5)$_3$·THF in CD_2Cl_2 at ambient temperature, following the procedure already established for the clean and quantitative generation of the analogous cationic species [((2,6-^{i}Pr$_2$C$_6$H$_3$)N=C(3,5-^{t}Bu$_2$C$_6$H$_2$)O)ZrBn$_2$(THF)]$^+$[BnB(C$_6$F$_5$)$_3$]$^-$.[61] In an argon-filled glovebox, a 4 mL glass vial was charged with 5.00 mg (6.00 μmol) of **1** and 0.4 mL of CD_2Cl_2, while another vial was charged with 3.50 mg of B(C_6F_5)$_3$·THF (6.00 μmol) and 0.4 mL of CD_2Cl_2. The two vials were mixed via pipet at ambient temperature to give instantaneously a pale yellow solution, and subsequent NMR analysis showed the clean and quantitative formation of ion pair **3**. (Note that NMR analysis must be finished within 15 min, as cation **3** starts to decompose at ambient temperature, as indicated by a color change from pale yellow to colorless after that period.)

^{1}H NMR (CD_2Cl_2, 23 °C): δ 7.71−7.67 (m, 1H, Ar-*H*), 7.57−7.50 (m, 3H, Ar-*H*), 7.46−7.33 (m, 4H, Ar-*H*), 7.27−7.11 (m, 6H, Ar-*H*, C_7H_8), 7.07−7.01 (m, 3H, Ar-*H*), 6.88−6.84 (m, 2H, Ar-*H*), 6.79−6.73 (m, 4H, Ar-*H*), 6.46−6.43 (m, 1H, Ar-*H*), 4.50−4.44 (m, 2H, Ar-CH_2NCH_2-Ar), 4.04−3.97 (m, 2H, Ar-CH_2NCH_2-Ar), 3.73 (bs, 2H, α-CH_2 of THF), 3.54 (bs, 2H, α-CH_2 of THF), 3.38 (s, 2H, NCH_2CH$_2$Ph), 2.86−2.70 (bs, 4H, Ar-CH_2-B, Ar-CH_2-Zr), 2.34 (s, 3H, C_7H_8), 1.81 (bs, 4H, β-CH_2 of THF), 1.56 (s, 9H, Ar-C(CH_3)$_3$), 1.49 (s, 2H, NCH$_2$CH_2Ph), 1.44 (s, 9H, Ar-C(CH_3)$_3$), 1.38 (s, 9H, Ar-C(CH_3)$_3$), 1.35 (s, 9H, Ar-C(CH_3)$_3$). ^{19}F NMR (CD_2Cl_2, 23 °C): δ −131.4 (m, 6F, *o*-F), −164.9 (t, J_{F-F} = 20.4 Hz, 3F, *p*-F), −167.7 (m, 6F, *m*-F).

In Situ Generation of {BnCH$_2$N[(2,4-^{t}Bu$_2$C$_6$H$_2$(CH$_2$)O]$_2$TiBn(THF)}$^+$[BnB(C$_6$F$_5$)$_3$]$^-$ (4). Cationic species **4** was generated by in situ mixing of **2** and B(C_6F_5)$_3$·THF in CD_2Cl_2 at ambient temperature, following the procedure already established for the clean and quantitative generation of the analogous cationic species [((2,6-^{i}Pr$_2$C$_6$H$_3$)N=C(3,5-^{t}Bu$_2$C$_6$H$_2$)O)ZrBn$_2$(THF)]$^+$[BnB(C$_6$F$_5$)$_3$]$^-$.[61] In an argon-filled glovebox, a 4 mL glass vial was charged with 10 mg (0.013 mmol) of **2** and 0.4 mL of CD_2Cl_2, while another vial was charged with 7.60 mg of B(C_6F_5)$_3$·THF (0.013 mmol) and 0.4 mL of CD_2Cl_2. The two vials were mixed via pipet at ambient temperature to give instantaneously a dark red solution, and subsequent NMR analysis showed the formation of ion pair **4**, accompanied by the decomposition products formed through the C_6F_5 ligand transfer from the borate anion to the Ti cation (see Results and Discussion).

^{1}H NMR (CD_2Cl_2, 23 °C): δ 7.58 (s, 1H, Ar-*H*), 7.54−7.44 (m, 4H, Ar-*H*), 7.37 (bs, 3H, Ar-*H*), 7.29−7.09 (m, 6H, Ar-*H*, C_7H_8), 7.06−6.95 (m, 3H, Ar-*H*), 6.88−6.85 (m, 2H, Ar-*H*), 6.79−6.73 (m, 4H, Ar-*H*), 6.46−6.38 (m, 1H, Ar-*H*), 4.25 (s, 1H, Ar-CH_2NCH_2-Ar), 3.95 (s, 1H, Ar-CH_2NCH_2-Ar), 3.79−3.64 (m, 4H, α-CH_2 of THF), 3.45−3.39 (m, 1H, Ar-CH_2NCH_2-Ar), 3.18−3.11 (m, 1H, Ar-CH_2NCH_2-Ar), 2.92 (NCH_2CH$_2$Ph), 2.85−2.75 (bs, 4H, Ar-CH_2-B, Ar-CH_2-Ti), 2.34 (s, 3H, C_7H_8), 2.04−1.86 (bs, 4H, β-CH_2 of THF), 1.78 (s, 9H, Ar-C(CH_3)$_3$), 1.64 (s, 9H, Ar-C(CH_3)$_3$), 1.56 (s, 2H, NCH$_2$CH_2Ph), 1.39 (s, 9H, Ar-C(CH_3)$_3$), 1.37 (s, 9H, Ar-C(CH_3)$_3$).

dx.doi.org/10.1021/om500661y | *Organometallics* 2014, 33, 4118−4130

Scheme 1. Protonolysis of MBn_4 with $N[(2,4\text{-}^tBu_2C_6H_2(CH_2)OH]_3$ Leading to Formation of the Unexpected C−C Bond Cleavage Product

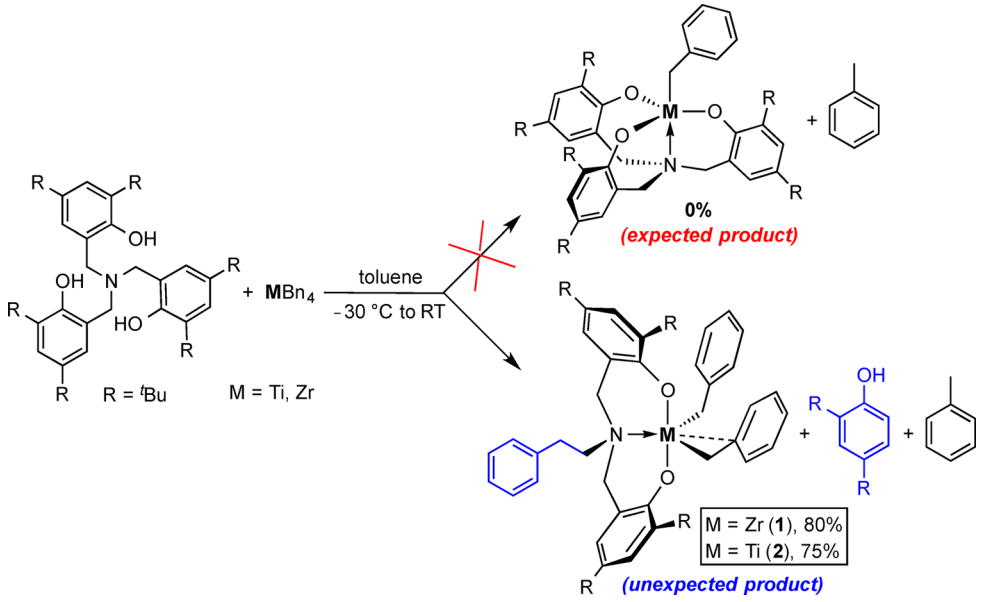

^{19}F NMR (CD_2Cl_2, 23 °C): δ −131.3 (m, 6F, *o*-F), −164.9 (t, J_{F-F} = 20.4 Hz, 3F, *p*-F), −167.7 (m, 6F, *m*-F).

General Polymerization Procedures. Polymerizations were performed in 30 mL glass reactors in the glovebox in toluene or CH_2Cl_2 at ambient temperature, following the procedure established for the polymerization of methacrylates and acrylamides by metallocene precatalysts.[67] In a typical in-reactor activation polymerization procedure, the activator $B(C_6F_5)_3$ (13.2 μmol) and 200 equiv (2.64 mmol) of $_\beta$MMBL (or $_\gamma$MMBL and MBL) were premixed in 3 mL of toluene or CH_2Cl_2 as indicated in the table. The polymerization was timed immediately after addition of a precatalyst. The preactivation method (i.e., premixing the neutral complex with an activator to generate the corresponding cationic catalyst, followed by addition of monomer to start the polymerization) was also adopted in some runs for comparison. Similar procedures were followed in the case of MMA polymerization. After the measured time interval, a 0.2 mL aliquot was taken from the reaction mixture via syringe and quickly quenched into a 4 mL vial containing 0.6 mL of undried "wet" $CDCl_3$ stabilized by 250 ppm of BHT-H; the quenched aliquots were later analyzed by ^1H NMR to obtain monomer conversion data. The polymerization was immediately quenched after the removal of the aliquot by adding 5 mL of 5% HCl-acidified methanol. The quenched mixture was precipitated into 100 mL of methanol, stirred for 3 h, filtered, and washed with methanol. The polymer collected was dried in a vacuum oven at 50 °C overnight to a constant weight.

Polymer Characterizations. Polymer number-average molecular weights (M_n) and molecular weight distributions (MWD = M_w/M_n) were measured by gel permeation chromatography (GPC) analyses carried out at 40 °C and a flow rate of 1.0 mL/min, with DMF (for PMBL and P_γMMBL samples) as the eluent, on a Waters University 1500 GPC instrument coupled with a Waters RI detector and equipped with four PLgel 5 μm mixed-C columns (Polymer Laboratories; linear range of molecular weight 200−2000000). The instrument was calibrated with 10 PMMA standards, and chromatograms were processed with Waters Empower software. ^{13}C NMR spectra for the analysis of PMBL,[9,24,28] P_γMMBL,[27,28] and P_βMMBL[16,15,36] microstructures were recorded and analyzed according to the cited literature methods.

Computational Methods. All of the density functional theory (DFT) calculations were performed using the Gaussian09 package and followed the procedures described in our prior publications.[68] The BP86 GGA functional of Becke and Perdew was used.[69,70] Geometry optimizations were performed with the standard split-valence basis set with a polarization function of Ahlrichs and co-workers for H, C, N, and O atoms (SVP keyword in Gaussian)[71] while the quasi-relativistic small-core Stuttgart ECP with the associated triple-ζ valence basis set was used for zirconium (SDD keyword in Gaussian09).[72] The reported energies have been obtained via single-point energy calculations with the BP86 and M06 functional with the triple-ζ basis set of Ahlrichs for H, C, N, and O (TZVP keyword in Gaussian09). Solvent (toluene) effects were included with the default Gaussian PCM implementation.[73] Thermal corrections from gas-phase frequency analysis, performed with the SVP basis set on the optimized geometries, were added to this in solvent energy to obtain the free energies.

RESULTS AND DISCUSSION

C−C Bond Cleavage in Protonolysis of MBn_4 with $N[(2,4\text{-}^tBu_2C_6H_2(CH_2)OH]_3$. It is well established that protonolysis of group 4 tetrakis(alkoxy) compounds $M(OR)_4$ with equimolar tetradentate amine-tris(phenol) ligands, such as $N[(2,4\text{-}^tBu_2C_6H_2(CH_2)OH]_3$, leads to the corresponding tripodal amine-tris(phenoxy) group 4 alkoxides $N[(2,4\text{-}^tBu_2C_6H_2(CH_2)O]_3M(OR)$, after concomitant elimination of 3 equiv of ROH.[63,74] In sharp contrast, protonolysis of group 4 tetrabenzyl complexes MBn_4 (M = Zr, Ti) with such a ligand in toluene from −30 to 25 °C unexpectedly afforded amine-bis(phenoxy) dibenzyl complexes **1** (M = Zr) and **2** (M = Ti) with concurrent liberation of the coproducts 2,4-di-*tert*-butylphenol and toluene (Scheme 1). The dibenzyl Zr and Ti complexes were both isolated in a pure state with good yields of 80% and 75%, respectively. Extended standing of Zr complex **1** at ambient temperature for longer than 48 h resulted in decomposition, but the compound can be stored inside a glovebox freezer at −35 °C without detectable decomposition for 2 months. Ti complex **2** is more sensitive to light, heat, and air/moisture; extended exposure to light and vacuum at ambient temperature even in the glovebox showed gradual decomposition.

The ^1H NMR spectrum of **1** (Figure 1, C_6D_6) and **2** showed that the benzylic CH_2 protons are diastereotopic, appearing as two sets of multiplets at δ 2.45−2.29 (in **1**) and 2.90−2.74 (in **2**). The chemical shifts revealed that the benzyl CH_2 groups in

dx.doi.org/10.1021/om500661y | *Organometallics* 2014, 33, 4118−4130

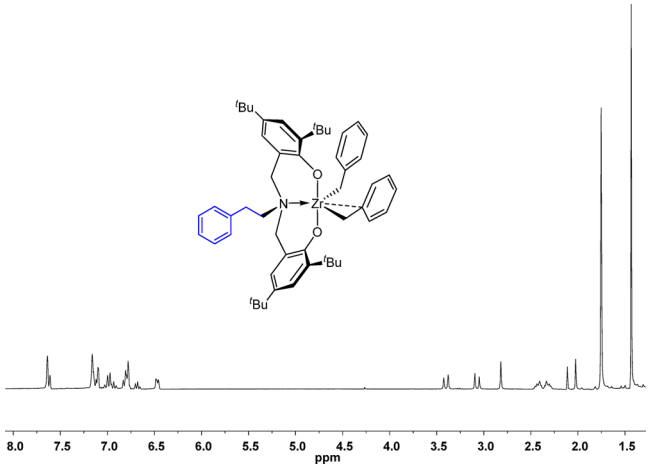

Figure 1. ^{1}H NMR (C_6D_6) spectrum of $BnCH_2N[(2,4\text{-}^tBu_2C_6H_2(CH_2)O]_2ZrBn_2$ (**1**).

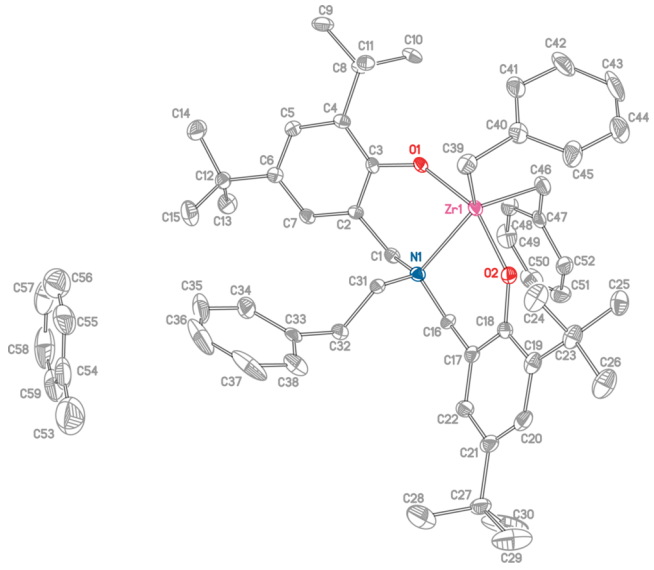

Figure 2. X-ray crystal structure of $BnCH_2N[(2,4\text{-}^tBu_2C_6H_2(CH_2)O]_2ZrBn_2$ (**1**) with thermal ellipsoids drawn at the 40% probability level. Selected bond lengths (Å) and angles (deg): Zr(1)−O(1), 1.989(2); Zr(1)−O(2), 1.996(2); Zr(1)−N(1), 2.377(3); Zr(1)−C(39), 2.288(4); Zr(1)−C(46), 2.272(3); Zr(1)−C(40), 2.680(3); C(31)−C(32), 1.532(4), N(1)−Zr(1)−C(39), 124.64(11), C(39)−Zr(1)−C(46), 118.94(13), C(46)−Zr(1)−N(1), 116.42(11), O(1)−Zr(1)−C(39), 94.35(11), O(1)−Zr(1)−C(46), 97.31(11), O(1)−Zr(1)−N(1), 79.17(9), O(2)−Zr(1)−C(39), 94.71(11), O(2)−Zr(1)−C(46), 96.87(11), O(2)−Zr(1)−N(1), 78.11(9), Zr(1)−C(39)−C(40), 88.2(2), Zr(1)−C(46)−C(47), 108.5(2); N(1)−C(31)−C(32), 115.6(3).

2 are slightly deshielded relative to those in **1**, which can be attributed to the weaker Lewis acidic Zr center in comparison to that of Ti. In addition, ^{13}C NMR spectra of **1** and **2** also revealed the benzyl $-CH_2$ groups in **2** (δ 85.8 for η^2-benzyl coordination ($^1J_{C-H}$ = 134.5 Hz), δ 84.1 for η^1-benzyl ($^1J_{C-H}$ = 130.9 Hz) coordination) are considerably more deshielded than the benzyl $-CH_2$ groups in **1** (δ 60.4 for η^1-benzyl coordination ($^1J_{C-H}$ = 128.8 Hz), δ 60.1 for η^2-benzyl coordination ($^1J_{C-H}$ = 137.7 Hz))[75] (cf. the crystal structure of **1** depicted in Figure 2). The four protons of the two benzyl $-CH_2$ groups in both **1** and **2** coalesced as a singlet in variable-temperature ^{1}H NMR (toluene-d_8) spectra at −20 °C (in **1**) and −60 °C (in **2**), thus indicating rapid interconversion of η^1 and η^2 benzyl coordination in solution at and above those coalescence temperatures. The two Ar-CH_2 protons in **1** appeared as two doublets (J = 12 Hz) at δ 3.40 and 3.07 ppm, respectively, while those in **2** showed two singlets at δ 3.79 and 3.63 ppm, consistent with a *mer* mode of coordination[76] between the amine-bis(phenoxyl) ligand and the metal. The resonances for the Ar-C(CH_3)$_3$) group, appearing as two singlets at δ 1.75 and 1.43 ppm in **1** and δ 2.07 and 1.43 ppm in **2**, are also indicative of the *mer* mode of coordination (four different resonances would be anticipated for a *fac* mode of coordination). The rest of the chemical shifts matched well with the related amine-bis(phenoxy) zirconium dibenzyl compound.[52]

Single-crystal X-ray diffraction analysis of **1** reveals that the Zr center exhibits a pentacoordinate, pseudo-trigonal-bipyramidal geometry (Figure 2), with two axial O atoms and equatorial [N,C,C] atoms—furnished with η^1 binding of one benzyl group, η^2 binding of the other benzyl group, and the datively bonded amido nitrogen—occupying all the coordination sites. The Zr−C(benzyl) distances, Zr(1)−C(39) = 2.288(4) Å and Zr(1)−C(46) = 2.272(3) Å, match well with those reported in the analogous complex $[(Pr)N\text{-}(2,4\text{-}^tBu_2C_6H_2(CH_2)O)_2]ZrBn_2$ (2.292(2), 2.272(2) Å).[52] The bond distance Zr(1)−N(1) = 2.377(3) Å represents a classical dative bond between N and Zr. The nonclassical η^2-bonded benzyl group is identified by the distance Zr(1)−C(40) = 2.680(3) Å and the acute bond angle Zr(1)−C(39)−C(40) = 88.2(2)°, presumably a result of electron deficiency at Zr and lack of steric crowding around the Zr center. On the other hand, the classical η^1-bonded benzyl group is readily identified by Zr(1)−C(47) = 3.08 Å and Zr(1)−C(46)−C(47) = 108.5°.

The acute bond angle Zr(1)−C(39)−C(40) and the obtuse bond angle Zr(1)−C(46)−C(47) show that the phenyl rings of both benzyl groups tilt toward the Zr center. Furthermore, the bond angles O(1)−Zr(1)−O(2) = 156.82(9)°, O(1)−Zr(1)−N(1) = 79.17(9)°, and O(2)−Zr(1)−N(1) = 78.11(9)° indicate the O atoms in the two phenoxy groups are nearly *trans* to each other. The equatorial coordination sites of the pseudo-trigonal-bipyramidal geometry are characterized by the obtuse bond angles N(1)−Zr(1)−C(39) = 124.64(11)°, C(39)−Zr(1)−C(46) = 118.94(13)°, and C(46)−Zr(1)−N(1) = 116.42(11)°, while the axial coordination sites are characterized by the bond angles O(1)−Zr(1)−C(39) = 94.35(11)°, O(1)−Zr(1)−C(46) = 97.31(11)°, O(1)−Zr(1)−N(1) = 79.17(9)°, O(2)−Zr(1)−C(39) = 94.71(11)°, O(2)−Zr(1)−C(46) = 96.87(11)°, and O(2)−Zr(1)−N(1) = 78.11(9)°, overall confirming the pseudo-trigonal-bipyramidal Zr center. Moreover, the bis(phenoxy)amine ligand is coordinated to Zr in a *mer* fashion,[76] with the amido N being placed at the equatorial position and the two O atoms of the phenoxy groups being placed at the axial positions, which is characterized by the angles O(1)−Zr(1)−O(2) = 156.82(9)°, O(1)−Zr(1)−N(1) = 79.17(9)°, and O(2)−Zr(1)−N(1) = 78.11(9)°.

Generation of Cationic Benzyl Complexes $\{BnCH_2N[(2,4\text{-}^tBu_2C_6H_2(CH_2)O]_2MBn(THF)\}^+[BnB(C_6F_5)_3]^-$ (M = Zr (3), Ti (4)). The stoichiometric reaction between dibenzyl **1** and $B(C_6F_5)_3$·THF in CD_2Cl_2 at room temperature led to the clean and quantitative formation of the corresponding ion pair $\{BnCH_2N[(2,4\text{-}^tBu_2C_6H_2(CH_2)O]_2ZrBn(THF)\}^+[BnB(C_6F_5)_3]^-$ (**3**) through benzyl abstraction by the borane (Scheme 2). The resulting free benzylborate anion [BnB-

dx.doi.org/10.1021/om500661y | *Organometallics* 2014, 33, 4118−4130

Scheme 2. Activation of the Dibenzyl Complexes To Generate Cationic Monobenzyl Complexes $\{BnCH_2N[(2,4\text{-}^tBu_2C_6H_2(CH_2)O]_2MBn(THF)\}^+[BnB(C_6F_5)_3]^-$

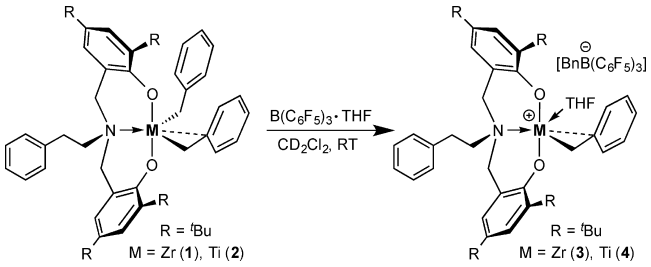

$(C_6F_5)_3]^-$ is readily characterized by its ^{19}F NMR resonances at δ −131.4 (m, 6F, *o*-F), −164.9 (t, 3F, *p*-F), and −167.7 (m, 6F, *m*-F), and the noncoordinating nature of the borate anion in **3** is established by ^{19}F NMR, in which a small chemical shift difference of <3 ppm (Δ(*m*,*p*-F) = 2.8 ppm in **3**) between the para and meta fluorines is diagnostic of the noncoordinating borate anion.[77] The freshly prepared ion pair solution is pale yellow, which turned colorless within 15 min at solution due to decomposition; standing of the CD_2Cl_2 solution for >1 h at room temperature resulted in complete decomposition. Attempts to generate the base-free cation using $B(C_6F_5)_3$ only led to unidentifiable products due to the decomposition. Thus, the Zr monobenzyl cation supported by the amine-bis(phenolate) ligand is stabilized via THF coordination[61] and η^2 coordination of the benzyl group to satisfy the octahedral coordination sites of Zr. We assumed that the presence of one η^2-bonded benzyl group satisfied the octahedral coordination sites of Zr, on the basis of the analogous cationic benzyl complexes $[((2,6\text{-}^iPr_2C_6H_3)N{=}C(3,5\text{-}^tBu_2C_6H_2)O)MBn_2(THF)]^+[BnB(C_6F_5)_3]^-$ (M = Zr, Ti), which were structurally characterized.[61] Furthermore, on the basis of literature precedents the group 4 cationic metal centers can be stabilized by η^6 coordination via π back-bonding of the abstracted benzyl group of the corresponding anion $[BnB(C_6F_5)_3]^-$,[78a,b] which is a potential coordination mode when a coordinating solvent such as THF is not accessible. ^1H NMR of **3** exhibited one diffuse broad signal for PhCH_2B and PhCH_2Zr at δ 2.70−2.86 ppm. The α-CH_2 group of the coordinated THF showed two broad signals at δ 3.54 and 3.73 ppm, while the respective β-CH_2 group showed one broad signal at δ 1.81 ppm. Four different singlets (δ 1.35, 1.38, 1.44, 1.56 ppm) observed for Ar-C(CH_3)$_3$ indicated the overall C_1 symmetry of the ion pair.

The cationic Ti species $\{BnCH_2N[(2,4\text{-}^tBu_2C_6H_2(CH_2)O]_2TiBn(THF)\}^+[BnB(C_6F_5)_3]^-$ (**4**) was generated in the same manner as for the generation of **3**, and the resulting free benzylborate anion $[BnB(C_6F_5)_3]^-$ was readily characterized by its ^{19}F NMR resonances at δ −131.3 (m, 6F, *o*-F), −164.9 (t, 3F, *p*-F), and −167.8 (m, *m*-F) ppm. However, in the case of the Ti cation **4**, its generation was accompanied by formation of two additional species, $BnCH_2N[(2,4\text{-}^tBu_2C_6H_2(CH_2)O]_2Ti(Bn)(C_6F_5)(THF)$ and $PhCH_2B(C_6F_5)_2$, due to decomposition via facile C_6F_5 ligand transfer to the cation from the borate anion.[78a,c,d] Thus, the Ti cation is even less thermally stable than the Zr cation, and standing of its CD_2Cl_2 solution at room temperature for 30 min resulted in complete decomposition.

Polymerization of $_\beta$MMBL and $_\gamma$MMBL. Control runs for the polymerization of $_\beta$MMBL (200:1) with the activator $B(C_6F_5)_3$ and neutral benzyl complexes (precatalysts **1**, **2**, **5**, and **6**) independently at room temperature in CH_2Cl_2 or toluene resulted in no polymer formation up to 24 h. On the other hand, their derived cationic complexes, upon appropriate activation, were found effective for the polymerization of $_\beta$MMBL, the results of which are summarized in Table 1.

Table 1. Selected Results of $_\beta$MMBL Polymerization[a]

run no.	complex	method	solvent	isolated yield (%)	[*rr*][b] (%)	[*mr*][b] (%)	[*mm*][b] (%)
1	**1**	A	toluene	26	n.d.	n.d.	n.d.
2	**1**	B	toluene	99	0.5	1.1	98.1
3	**2**	A	toluene	30	0.3	3.5	96.2
4	**2**	B	toluene	70	1.6	0.1	98.1
5	**2**	A	CH_2Cl_2	10	n.d.	n.d.	n.d.
6	**5**	A	toluene	70	0.1	3.6	96.2
7	**5**	B	toluene	99			99.0
8	**5**	A	CH_2Cl_2	18	n.d.	n.d.	n.d.
9	**6**	B	toluene	21	0.9	4.5	94.3

[a]Conditions: [$_\beta$MMBL]/[complex]/[$B(C_6F_5)_3$], 200/1/1; solvent, 3 mL; temperature, 25 °C; time, 24 h; n.d., not determined. Method A: preactivation (premixing the neutral complex with the activator to generate the corresponding cationic catalyst, followed by addition of monomer to start the polymerization). Method B: in-reactor activation (premixing the monomer with the activator, followed by addition of the neutral complex). [b]Tacticity measured by ^{13}C NMR spectroscopy with TFA-*d* as a solvent at 70 °C.

Typically, the coordination−addition polymerization of acrylic monomers using cationic group 4 metallocenium complexes are performed in the relatively nonpolar hydrocarbon solvent toluene or the polar noncoordinating solvent CH_2Cl_2, while polar coordinating solvents such as THF and DMF usually suppress the polymerization due to their strong coordination to the highly electron deficient metal center.[35] Accordingly, toluene and CH_2Cl_2 were used for this polymerization study.

Using the preactivation protocol that pregenerates the cationic catalyst (method A), the polymerization of $_\beta$MMBL in toluene by the Zr complex **1** (0.5 mol %) and $B(C_6F_5)_3$ achieved only 26% yield (run 1, Table 1). On the other hand, the in-reactor activation protocol (method B) afforded quantitative monomer conversion (99% isolated polymer yield, run 2). The observed large yield difference between the two activation methods reaffirmed the results of the activation study described above that the cationic species is unstable in the absence of monomer. Most significantly, solubility tests showed that the resulting polymer P$_\beta$MMBL is insoluble in common organic solvents such as $CHCl_3$, THF, DMF, DMSO, acetonitrile, and dichlorobenzene, at room temperature or under reflux conditions. This insolubility limited the ability to measure the molecular weight of P$_\beta$MMBL by GPC analysis, but it strongly suggests that the resulting polymer is highly stereoregular.[16,15,36] Indeed, analysis of the resulting P$_\beta$MMBL by ^{13}C NMR in TFA-*d* as a solvent at 70 °C showed the polymer is *highly isotactic* with 98.1% *mm* (run 2, Figure 3).

Likewise, the polymerization of $_\beta$MMBL in toluene by the Ti complex **2** and $B(C_6F_5)_3$ using method A achieved only 30% polymer yield (run 3), while method B resulted in 70% isolated polymer yield (run 4), although the resulting polymers by both methods are highly isotactic with 96−98% *mm*. Owing to the instability of the preformed cation in CH_2Cl_2 in the absence of monomer, the polymerization of $_\beta$MMBL in this solvent using method A gave only 10% isolated yield (run 5).

dx.doi.org/10.1021/om500661y | *Organometallics* 2014, 33, 4118−4130

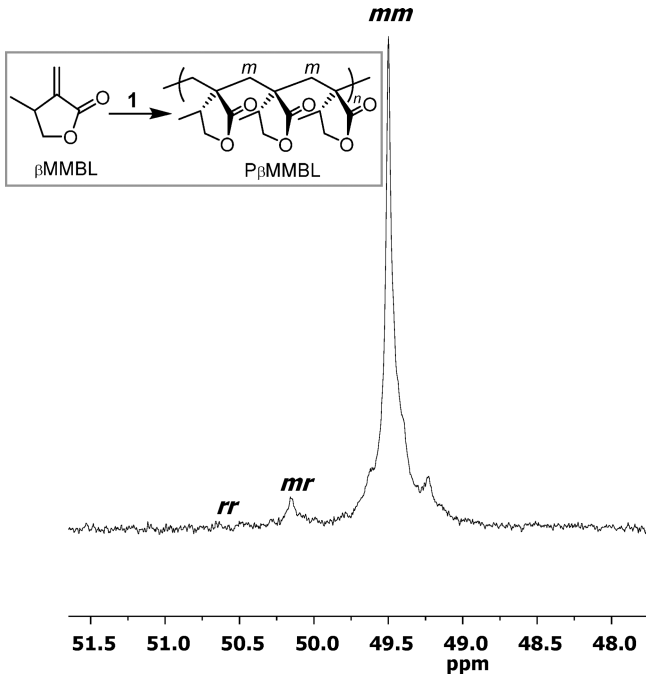

Figure 3. ^{13}C NMR (125 MHz, TFA-*d*, 70 °C) of the isotactic P$_\beta$MMBL (98% *mm*) produced by complex **1** (run 2, Table 1) in the backbone quaternary carbon (*rr*, *mr*, *mm*) region.

To examine the generality of isospecific polymerization of $_\beta$MMBL by coordination polymerization catalysts, we extended this investigation by including the two previously reported (imino)phenoxy benzyl complexes **5**[61] and **6**[61] for polymerization of $_\beta$MMBL. The polymerization results (runs 6–9) showed a similar trend in the activity and isospecificity of the $_\beta$MMBL polymerization. In particular, the polymerization of $_\beta$MMBL by **5** using the in-reactor activation protocol gave a 99% isolated yield of P$_\beta$MMBL that exhibited >99% *mm* (run 7). Overall, the polymerization by the precatalyst using the in-reactor activation protocol gave better polymerization activity in comparison to the preactivation protocol, which is especially important for the cations having limited stability in the absence of monomer. Regarding the high isotacticity of P$_\beta$MMBL achieved by the current catalyst system, the stereocontrol mechanism should follow the path we already elucidated for the coordination polymerization of $_\beta$MMBL.[15,36] Specifically, the predominant chain-end stereocontrol in the coordination–addition polymerization of $_\beta$MMBL, which forms an isotactic polymer, chiefly originates from steric interactions between the methyl groups on the chiral β-C atom of the five-membered ring of both the coordinated $_\beta$MMBL and the last inserted $_\beta$MMBL unit of the chain.

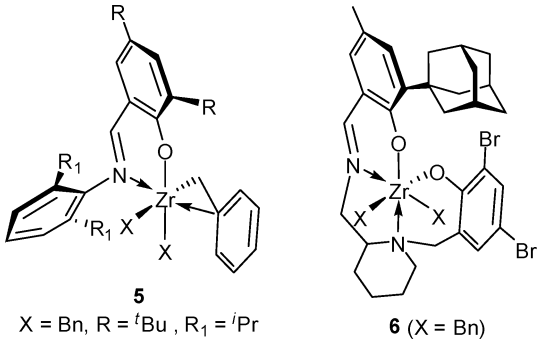

Employing the superior in-reactor activation protocol with $B(C_6F_5)_3$, complexes **1** and **2** were also investigated for their performance in the polymerization of $_\gamma$MMBL (200–400 equiv) at room temperature in toluene, the results of which were summarized in Table 2. With a 0.5 mol % precatalyst loading, near-quantitative monomer conversion (98% isolated polymer yield) was achieved (run 1, Table 2). The resulting P$_\gamma$MMBL showed a measured M_n value of 6.13 × 10^4 g/mol and a molecular weight distribution of 1.97. Lowering the precatalyst loading to 0.25 mol % (i.e., raising the [$_\gamma$MMBL]/[**1**] ratio to 400) still afforded a high polymer yield of 93%, but predictably, the resulting P$_\gamma$MMBL had a much higher molecular weight of M_n = 9.26 × 10^4 (run 2, Table 2). The polymerization by the Ti precatalyst **2** with a 0.5 mol % loading performed comparably to that of the Zr precatalyst **1** (run 3 vs run 1, Table 2), but the Ti catalyst achieved only a modest polymer yield of 65% when the precatalyst loading was lowered to 0.25 mol % (run 4, Table 2). However, regardless of the type and loading of the precatalyst, all of the resulting polymers were essentially atactic with [*mr*] values ranging from 40 to 47%. The challenge to control the stereochemistry of $_\gamma$MMBL polymerization is well-known in the literature. For example, $_\gamma$MMBL polymerization by the catalyst derived from [*rac*-$C_2H_4(\eta^5$-indenyl)$_2$]ZrMe[OC(O^{i}Pr)=CMe$_2$], which has shown to be highly isospecific for MMA and $_\beta$MMBL polymerizations,[36] produced only an atactic P$_\gamma$MMBL (42.4 *mr*).

Mechanism of Protonolysis Leading to C–C Bond Cleavage Products 1 and 2. MBn$_4$ (M = Zr, Ti) upon protonolysis with equimolar N[(2,4-^{t}Bu$_2$C$_6$H$_2$(CH$_2$)OH]$_3$ in toluene from −30 to 25 °C afforded unexpectedly amine-bis(phenoxy) dibenzyl complexes **1** (M = Zr) and **2** (M = Ti) with concurrent liberation of the coproducts 2,4-di-*tert*-butylphenol and toluene (Scheme 1), instead of the expected tripodal amine-tris(phenoxy) monobenzyl complexes N-[(2,4-^{t}Bu$_2$C$_6$H$_2$(CH$_2$)O]$_3$MBn if the reaction involved only protonolysis but no C–C bond cleavage. One of the possible mechanisms for the formation of such C–C bond cleavage products involves radical intermediates due to photochemical

Table 2. Selected Results of $_\gamma$MMBL Polymerization by Precatalysts 1 and 2[a]

run no.	complex	monomer/complex	isolated yield (%)	$10^{-4}M_n$[b]	PDI[b] (M_w/M_n)	[*rr*][c] (%)	[*mr*][c] (%)	[*mm*][c] (%)
1	**1**	200	98	6.13	1.97	46.5	44.4	9.1
2	**1**	400	93	9.26	2.35	42.0	47.0	11.0
3	**2**	200	97	4.63	1.82	35.0	47.0	18.0
4	**2**	400	65	6.00	2.03	48.0	40.2	11.8

[a]Conditions: [complex]/[$B(C_6F_5)_3$], 1; solvent, 3 mL (toluene); temperature, 25 °C; time, 24 h; monomer was premixed with the activator $B(C_6F_5)_3$ followed by addition of complex (i.e., in-reactor activation). [b]Number-average molecular weight (M_n) and polydispersity index (PDI) determined by GPC relative to PMMA standards. [c]Tacticity measured by ^{13}C NMR spectroscopy with DMSO-d_6 as solvent at 100 °C.

dx.doi.org/10.1021/om500661y | *Organometallics* 2014, 33, 4118–4130

Scheme 3. Comparison of Energetics (kcal/mol) Involved in the Reaction of I with [O_3N] To Form II and III[a]

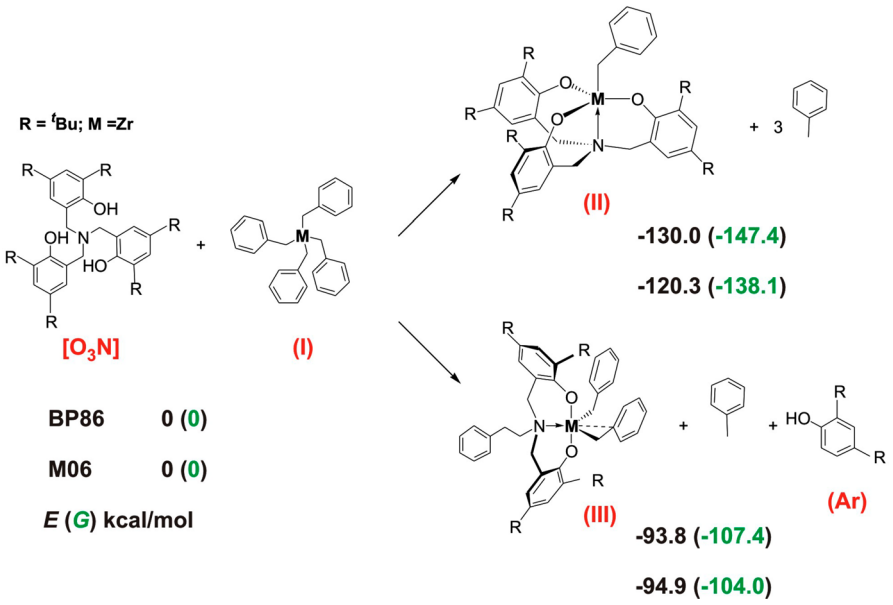

[a]Values in black and in green correspond to internal and free energies in toluene, obtained with the BP86 and M06 functionals.

Scheme 4. Reaction Pathway and Energetics (kcal/mol) Involved in the Formation of II[a]

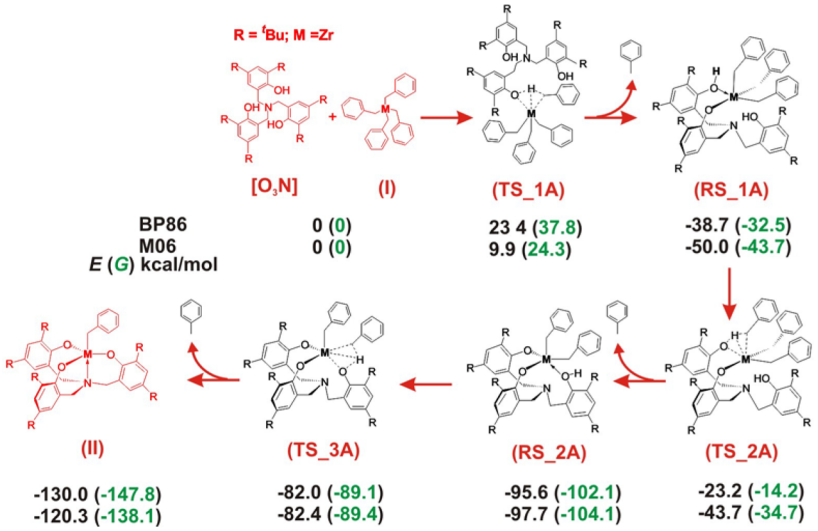

[a]Values in black and in green correspond to internal and free energies in toluene, obtained with the BP86 and M06 functionals.

decomposition of the precursor MBn_4 to the tribenzyl metal(III) complex and the benzyl radicals,[62] even though the current reaction was performed in a glass reactor wrapped with Al foil to minimize exposure to light. Photolysis of MBn_4 was reported to proceed more quickly in ethers and aromatic hydrocarbons than in aliphatic hydrocarbons.[62a] These precursors are unstable in toluene solution, and the decomposition rate increases with the temperature (a typical lifetime of $TiBn_4$ in toluene solution is 8 h; the presence of light changes the color of $ZrBn_4$ in solution from yellow to brown even at temperatures at which no thermal decomposition occurs).[62a] We reasoned that, since the lifetime and decomposition rate of such precursors are sensitive to solvent, light, and temperature, the results from investigations into effects of solvent, light, and temperature on the formation of amine-bis(phenoxy) dibenzyl complex **1** should provide evidence to argue for or against the hypothesis for the benzyl radical and tribenzyl metal(III) complex involvement in the above reaction.

Accordingly, we performed three additional sets of experiments on protonolysis of $ZrBn_4$ with $N[(2,4\text{-}^tBu_2C_6H_2(CH_2)\text{-}OH]_3$ by varying factors such as solvent, light, and heat. The first set of experiments involved the reaction in diethyl ether that was performed in a glass reactor wrapped with Al foil to minimize exposure to light; this condition increased the selectivity for complex **1** (89% yield), as compared to that performed in toluene (80% yield) under otherwise identical conditions. In contrast, switching the solvent to hexanes decreased the selectivity for complex **1** (55% yield; ^{1}H NMR analysis of the crude reaction mixture showed the presence of the unreacted ligand and other unidentified byproducts). These results from the above investigations into solvent effects

dx.doi.org/10.1021/om500661y | Organometallics 2014, 33, 4118−4130

seemed to support the role of photolysis of MBn_4 under the reaction conditions and thus the direct involvement of the resulting benzyl radicals and trivalent tribenzyl Zr complex in the formation of **1**. Additional support for this hypothesis was provided by a second set of experiments that performed the protonolysis reaction in toluene in a reactor directly exposed to light (i.e., no wrapping with Al foil); this condition led to an increased selectivity for complex **1** formation (87% yield), in comparison to that (80% yield) performed in toluene under minimum light exposure using Al foil wrapping. Finally, when the protonolysis reaction was performed in toluene at 80 °C under light, unidentifiable compounds were formed, due to thermal and photochemical decomposition of the precursor $ZrBn_4$ and the product **1**. Overall, all of the above three sets of the experiments investigating the effects of solvent, light, and heat supported the hypothesis for the involvement of the benzyl radicals and the trivalent Zr(III) complex resulting from thermal and photochemical decomposition of the precursor $ZrBn_4$.

DFT calculations were performed on the protonolysis reaction of tetrabenzylzirconium complex (**I**) with tridentate phenol $N[(2,4\text{-}^tBu_2C_6H_2(CH_2)OH)]_3$ ($[O_3N]$) to rationalize the formation of bis(phenoxy)-dibenzyl complex $C_6H_5\text{-}CH_2N\text{-}(CH_2\text{-}2,4\text{-}^tBu_2\text{-}C_6H_2\text{-}O)_2Zr(CH_2\text{-}C_6H_5)_2$ (**III**), instead of the tris(phenoxy)-monobenzyl complex $N(CH_2\text{-}2,4\text{-}^tBu_2\text{-}C_6H_2\text{-}O)_3Zr(CH_2\text{-}C_6H_5)$ (**II**), as expected on the basis of the analogous reactions with a Zr tetraalkoxide precursor[74] (Scheme 3). The internal energy (E) and the free energy (G) reported herein were obtained with the BP86 and M06 functionals. In both cases the effects of solvent (toluene) were considered.

As shown in Scheme 3, calculations revealed that formation of the expected tris(phenoxy)-monobenzyl complex **II** is favored by about 30−40 kcal/mol relative to the actually obtained complex **III**, in terms of internal energy and free energy as well, with both functionals. Subsequently, we focused our attention on the possible mechanisms leading to complexes **II** and **III**. Scheme 4 depicts the possible reaction pathway and the energies involved in the formation of the tris(phenoxy)-monobenzyl complex **II**.

The reaction involves three consecutive toluene elimination steps leading to the mono(phenoxy)-tribenzyl complex **RS_1A**, to the bis(phenoxy)-dibenzyl complex **RS_2A**, and finally to the tris(phenoxy)-monobenzyl complex **II**, respectively. As shown in Scheme 4, the rate-determining step is the first elimination reaction, showing a transition state that, in terms of internal energy, is 23.4 and 9.9 kcal/mol above the reactants at the BP86 and M06 levels, respectively. In terms of free energy the TS is 10 kcal/mol higher in energy, with both functionals due to an unfavored entropic contribution, a consequence of the bimolecular character of this reaction step. The first elimination product is about −40 and −50 kcal/mol below the reactants at the BP86 and M06 levels. Similar energy gains were observed for the successive elimination products generated through TSs that show energetic barriers not exceeding 10 kcal/mol in terms of both free energy and internal energy with both functionals considered (Scheme 4).

To rationalize the formation of the bis(phenoxy)-dibenzyl complex **III**, we examined several possible reaction pathways. As we were not able to find an energetically feasible mechanism mediated directly by Zr(IV) complexes, we focused on possible reaction mechanisms where the active metal species is a Zr(III) species, considering the well-known, facile photochemical decomposition of tetrabenzylzirconium to tribenzylzirconium with formation of benzyl radicals.[62] As the first step, we performed time-dependent DFT calculations (TDDFT) to investigate the possible photochemical decomposition of $ZrBn_4$. The energetics involved in this reaction is reported in Figure 4.

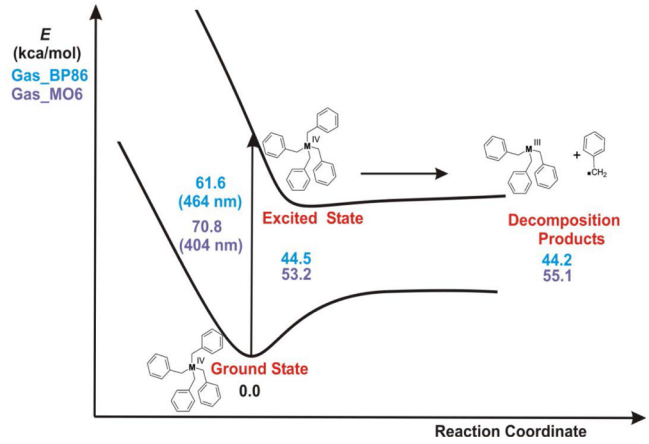

Figure 4. *Illustrative* potential energy curves for the $ZrBn_4$ ground state and the first singlet excited state with the energetics (kcal/mol) involved in the corresponding vertical transition and in the following $ZrBn_3$ plus benzyl radical formation. The values were calculated with the BP86 (green) and M06 (purple) functionals in the gas phase.

As expected, the absorption band for the transition from the ground-state singlet, 464 and 404 nm at the BP86 and M06 levels, is in the visible region. The optimized singlet excited state, as well as the dissociated tribenzylzirconium plus benzyl radical decomposition products, are almost at the same energy, about 50 kcal/mol from the ground state.[79] This indicates that inclusion of entropy should facilitate decomposition of $ZrBn_4$ after excitation of the complex to the first singlet excited state. Accordingly, we decided to investigate reaction pathways involving radical intermediates. The most reasonable mechanism we found for explaining formation of complex **III** is reported in Scheme 5.

The reaction starts with coordination of one phenol oxygen of the tridentate ligand $[O_3N]$ to the tribenzyl-Zr(III) complex to form coordination intermediate **1B**, which undergoes protonolysis with elimination of toluene and formation of the mono(phenoxy)-dibenzyl intermediate **RS_1B**. The energy barrier of this first step is about 15 kcal/mol with both of the functionals considered. Intermediate **RS_1B**, which is remarkably lower in energy than the reactants, shows an interaction between a second phenol oxygen of the ligand and the metal. However, calculations suggest that, instead of elimination of a second toluene molecule through the protonolysis transition state **TS_2B′**, intermediate **RS_1B** collapses into the clearly more stable intermediate **RS_2B**, where the two phenols of the ligand interact with the Zr, one of them interacting through the carbonyl oxygen of its tautomeric keto form (Scheme 5). The geometries of **RS_1B** and **RS_2B**, depicted in Figure 5, indicate that the sp^3 C_α (**RS_2B**) determines the conformation of the phenol ring that allows the coordination of the oxygen of a third phenol to the Zr(III). Additional coordination of the third phenol is prevented for steric reasons when both phenols of the ligand are in the enol form, as in **RS_1B**.

From intermediate **RS_2B** we hypothesized two TSs involving a H transfer from one O atom to the ring of the

dx.doi.org/10.1021/om500661y | *Organometallics* 2014, 33, 4118−4130

Scheme 5. Reaction Pathways and Energetics (kcal/mol) Involved in the Proposed Mechanism for the Formation of III[a]

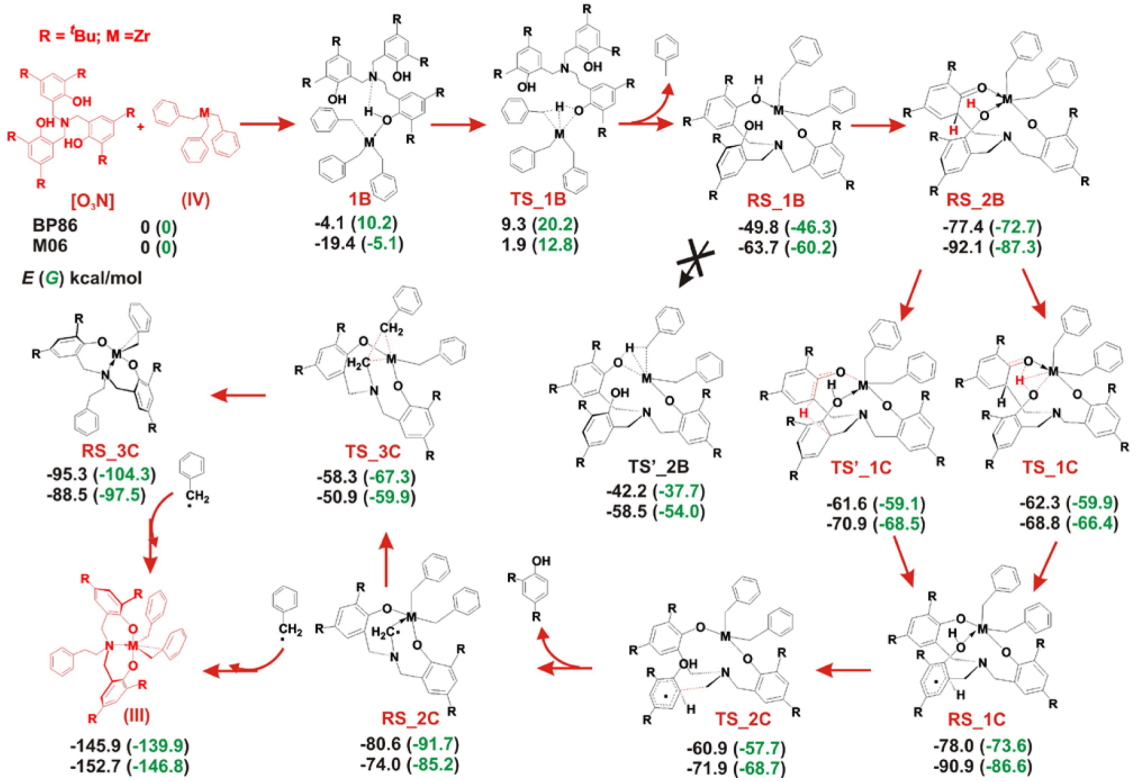

[a]Values in black and in green correspond to internal and free energies in toluene, obtained with the BP86 and M06 functionals.

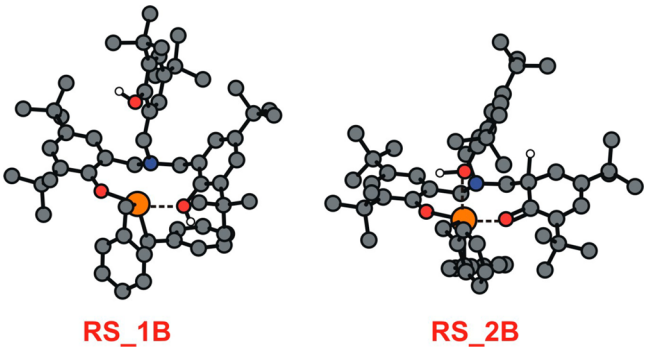

Figure 5. Comparison between **RS_1B** and **RS_2B** geometries.

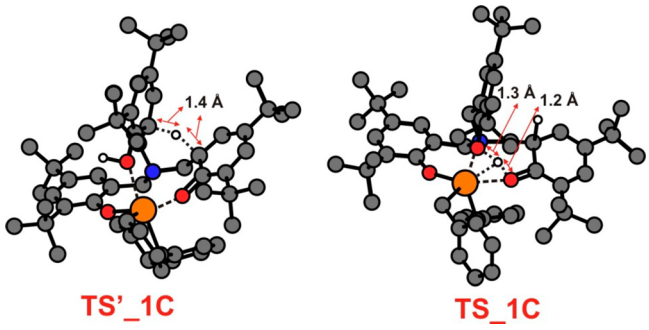

Figure 6. Comparison between the geometries of transition states **TS′_1C** and **TS_1C** for H-transfer.

phenol which results in the oxidation of the Zr, in the formation of a new Zr−O bond, and in delocalization of the radical onto one of the phenol ring of the ligand **RS_1C**. Transition state **TS′_1C** involves transfer of the α-hydrogen of the phenol in the keto form to the C_α of the nearby phenol in the enol form of the ligand (Figure 6), whereas in transition state **TS_1C** the hydrogen of the hydroxyl group of the phenol in the enol form is transferred to the carbonyl oxygen of the nearby phenol in the keto form. While the H transfer in transition state **TS′_1C** is direct, in transition state **TS_1C** it is mediated by the metal.

The H-transfer reaction can occur through both TSs, since no meaningful energy difference between the two TSs was found, independent of the functional considered. This H-transfer reaction shows an energy barrier of about 15−20 kcal/mol, depending on the specific functional considered.[80] Moreover, since intermediate **RS_1C** is isoenergetic with intermediate **RS_2B** with both functionals, the H-transfer reaction is an equilibrium reaction. The driving force of the reaction is the successive elimination of the experimentally observed 2,4-$tBu_2C_6H_3$-OH (Ar) which occurs through transition state **TS_1C** with an energy barrier of about 18 kcal/mol and formation of intermediate **RS_2C**. This intermediate shows an interaction of the methylenic carbon bonded to the nitrogen atom of the ligand with the Zr center and it is about 20 kcal/mol more stable than **RS_1C** at the BP86 level.

Finally, we considered two pathways that start from the radical **RS_2C** intermediate for the formation of the experimentally observed complex **III**: one proceeds via intermolecular radical coupling involving the radical **RS_2C** and the benzyl radical formed in the decomposition reaction of $ZrBn_4$. The other is an intramolecular reaction involving one benzyl group bonded to the Zr in **RS_2C** to form intermediate **RS_3C**, which lies about 15 kcal/mol lower in energy. This reaction proceeds through transition state **TS_3C**, with an energy barrier of about 20 kcal/mol (with both functionals).

dx.doi.org/10.1021/om500661y | *Organometallics* 2014, 33, 4118−4130

Complex **III** is finally formed by coupling of **RS_3C** with the benzyl radical (Scheme 5).

CONCLUSIONS

In summary, we have discovered an unusual C−C bond cleavage in the protonolysis of group 4 tetrabenzyl complexes MBn_4 (M = Zr, Ti) with the tetradentate amine-tris(phenol) ligand $N[(2,4\text{-}^tBu_2C_6H_2(CH_2)OH]_3$, resulting in the formation of the unexpected amine-bis(phenoxy) dibenzyl complexes **1** (80% isolated yield) and **2** (75% isolated yield) with concurrent liberation of the coproducts 2,4-di-*tert*-butylphenol and toluene. The molecular structure of the Zr complex **1** has been confirmed by X-ray diffraction analysis, featuring a pentacoordinate, pseudo-trigonal-bipyramidal geometry at Zr, which is coordinated by the amine-bis(phenoxy) ligand in a *mer* fashion, with two axial O atoms and equatorial [N,C,C] atoms—furnished with η^1 binding of one benzyl group, η^2 binding of the other benzyl group, and a datively bonded amido nitrogen.

Activation of the dibenzyl Zr complex **1** with $B(C_6F_5)_3$·THF in CD_2Cl_2 at room temperature generated cleanly and quantitatively the corresponding cationic complex **3** through benzyl abstraction by the borane. The analogous abstractive reaction with the Ti dibenzyl complex **2** was less clean and was accompanied by the two byproducts as a result of transfer of the C_6F_5 ligand transfer from the anion to the cation due to the instability of the Ti cation **4**. The in situ generated Zr cation **3** through the in-reactor activation protocol promoted highly stereospecific polymerization of the biomass-derived renewable monomer $_\beta$MMBL into the highly isotactic polymer P$_\beta$MMBL with 98.1% *mm* and quantitative yield. The analogous Ti cation **4** was less effective in terms of polymer yield, but the tacticity of the resulting polymer is similar. Both cationic complexes are also effective for polymerization of $_\gamma$MMBL, leading to essentially atactic P$_\gamma$MMBL.

Experimental studies in probing a possible mechanistic pathway for the observed unusual C−C bond cleavage in the present protonolysis reaction between $ZrBn_4$ and $N[(2,4\text{-}^tBu_2C_6H_2(CH_2)OH]_3$ for the formation of complex **1** investigated the effects of solvent, light, and heat on the reaction outcome. Overall, the experimental results appeared to support the hypothesis for the involvement of the benzyl radicals and the trivalent Zr(III) complex resulting from thermal and photochemical decomposition of the precursor $ZrBn_4$. DFT calculations were also performed on the protonolysis reaction. The mechanistic scenario that emerged from the computational study suggested that the reaction starts with coordination of one phenol oxygen of the tridentate ligand $[O_3N]$ to tribenzyl-Zr(III) to form the mono(phenoxy)-dibenzyl intermediate as a result of a protonolysis reaction with elimination of toluene. This intermediate carries two phenols of the ligand that interact with the Zr, one of them through the carbonyl oxygen of its tautomeric keto form. Through a H-transfer from one O atom to the ring of the phenol, oxidation of the Zr center in this intermediate occurs to form a new Zr−O σ-bond. The corresponding intermediate barriers the delocalized radical on one phenol ring of the ligand. Therefore, a bis(phenoxy)-dibenzyl radical intermediate, with the unpaired electron essentially delocalized on the ring of the last added phenol, is formed. The reaction proceeds through the energetically favored elimination of 2,4-di-*tert*-butylphenol to form a bis(phenoxy)-dibenzyl radical intermediate, where the methylenic carbon bonded to the nitrogen of the ligand interacts with the metal. Finally, the amine-bis(phenoxy) dibenzyl complex, $BnCH_2N[(2,4\text{-}tBu_2C_6H_2(CH_2)O]_2ZrBn_2$, is formed either through an intermolecular radical coupling involving the benzyl radical present in the reaction medium as result of the decomposition of $ZrBn_4$, or through an intramolecular reaction involving one benzyl group bonded to the Zr, followed by radical coupling with the benzyl radical.

ASSOCIATED CONTENT

Supporting Information

Text, tables, figures, and CIF and xyz files giving single-crystal X-ray diffraction data for **1** and computational details. This material is available free of charge via the Internet at http://pubs.acs.org.

AUTHOR INFORMATION

Corresponding Authors

*E-mail for L.C.: lcaporaso@unisa.it.

*E-mail for E.Y.-X.C.: eugene.chen@colostate.edu.

Notes

The authors declare no competing financial interest.

ACKNOWLEDGMENTS

This work was supported by the National Science Foundation (NSF-1300267) for the study carried out at Colorado State University. L.C. thanks the HPC team of Enea (www.enea.it) for using the ENEA-GRID and the HPC facilities CRESCO (www.cresco.enea.it) in Portici, Italy. We thank Boulder Scientific Co. for the research gift of $B(C_6F_5)_3$ and Dr. Brian Newell for assistance on X-ray structural analysis.

REFERENCES

(1) Gowda, R. R.; Chen, E. Y.-X. Sustainable Polymers from Biomass-Derived α-Methylene-γ-Butyrolactones. *Encycl. Polym. Sci. Technol.* **2013**, DOI: 10.1002/0471440264.pst606.

(2) Williams, C. K.; Hillmyer, M. A. Polymers from Renewable Resources: A Perspective for a Special Issue of Polymer Reviews. *Polym. Rev.* **2008**, *48*, 1−10.

(3) Meier, M. A. R.; Metzger, J. O.; Schubert, U. S. Plant Oil Renewable Resources as Green alternatives in Polymer Science. *Chem. Soc. Rev.* **2007**, *36*, 1788−1802.

(4) Coates, G. W.; Hillmyer, M. A. A virtual issue on "Polymers from Renewable Resources". *Macromolecules* **2009**, *42*, 7987−7989.

(5) Gandini, A. Polymers from Renewable Resources: a Challenge for the Future of Macromolecular Materials. *Macromolecules* **2008**, *41*, 9491−9504.

(6) Tullo, A. H. Growing Plastics. *Chem. Eng. News* **2008**, *86* (39), 21−25.

(7) Rossum, M. W. P. C. V.; Alberda, M.; Plas, L. H. W. V. D. *Phytochemistry* **1998**, *49*, 723−729.

(8) Reviews: (a) Kitson, R. R. A.; Millemaggi, A.; Taylor, R. J. K. *Angew. Chem., Int. Ed.* **2009**, *48*, 9426−9451. (b) Hoffman, H. M. R.; Rabe, J. *Angew. Chem., Int. Ed.* **1985**, *24*, 94−110.

(9) Akkapeddi, M. K. *Macromolecules* **1979**, *12*, 546−551.

(10) Brandenburg, C. J. U.S. Patent 6841627 B2, 2005.

(11) Pickett, J. E.; Ye, Q. U.S. Patent 2007/0122625, 2007.

(12) Manzer, L. E. *ACS Symp. Ser.* **2006**, *921*, 40−51.

(13) Manzer, L. E. *Appl. Catal. A: Gen.* **2004**, *272*, 249−256.

(14) Pittman, C. U., Jr.; Lee, H. *J. Polym. Sci., Part A: Polym. Chem.* **2003**, *41*, 1759−1777.

(15) Hu, Y.; Wang, X.; Chen, Y.; Caporaso, L.; Cavallo, L.; Chen, E. Y.-X. *Organometallics* **2013**, *32*, 1459−1465.

(16) Hu, Y.; Miyake, G. M.; Wang, B.; Cui, D.; Chen, E. Y.-X. *Chem. Eur. J.* **2012**, *18*, 3345−3354.

(17) Gowda, R. R.; Chen, E. Y.-X. *Org. Chem. Front.* **2014**, *1*, 230−234.

(18) Akkapeddi, M. K. *Polymer* **1979**, *20*, 1215−1216.
(19) Stansbury, J. W.; Antonucci, J. M. *Dent. Mater.* **1992**, *8*, 270−273.
(20) Mosnáček, J.; Yoon, J. A.; Juhari, A.; Koynov, K.; Matyjaszewski, K. *Polymer* **2009**, *50*, 2087−2094.
(21) Mosnáček, J.; Matyjaszewski, K. *Macromolecules* **2008**, *41*, 5509−5511.
(22) Ueda, M.; Takahashi, M.; Imai, Y.; Pittman, C. U., Jr. *J. Polym. Sci., Polym. Chem. Ed.* **1982**, *20*, 2819−2828.
(23) Gridnev, A. A.; Ittel, S. D. Patent WO035960 A2, 2000.
(24) Sogah, D. Y.; Hertler, W. R.; Webster, O. W.; Cohen, G. M. *Macromolecules* **1987**, *20*, 1473−1488.
(25) Miyake, G. M.; Newton, S. E.; Mariott, W. R.; Chen, E. Y.-X. *Dalton Trans.* **2010**, *39*, 6710−6718.
(26) Qi, G.; Nolan, M.; Schork, F. J.; Jones, C. W. *J. Polym. Sci., Polym. Chem.* **2008**, *46*, 5929−5944.
(27) Suenaga, J.; Sutherlin, D. M.; Stille, J. K. *Macromolecules* **1984**, *17*, 2913−2916.
(28) Zhang, Y.; Schmitt, M.; Falivene, L.; Caporaso, L.; Cavallo, L.; Chen, E. Y.-X. *J. Am. Chem. Soc.* **2013**, *135*, 17925−17942.
(29) Miyake, G. M.; Zhang, Y.; Chen, E. Y.-X. *Macromolecules* **2010**, *43*, 4902−4908.
(30) Hu, Y.; Xu, X.; Zhang, Y.; Chen, Y.; Chen, E. Y.-X. *Macromolecules* **2010**, *43*, 9328−9336.
(31) Zhang, Y.; Miyake, G. M.; Chen, E. Y.-X. *Angew. Chem., Int. Ed.* **2010**, *49*, 10158−10162.
(32) Zhang, Y.; Miyake, G. M.; John, M. G.; Falivene, L.; Caporaso, L.; Cavallo, L.; Chen, E. Y.-X. *Dalton Trans.* **2012**, *41*, 9119−9134.
(33) Zhang, Y.; Chen, E. Y.-X. *Angew. Chem., Int. Ed.* **2012**, *51*, 2465−2469.
(34) Zhang, Y.; Gustafson, L. O.; Chen, E. Y.-X. *J. Am. Chem. Soc.* **2011**, *133*, 13674−13684.
(35) Chen, E. Y.-X. *Chem. Rev.* **2009**, *109*, 5157−5214.
(36) Chen, X.; Caporaso, L.; Cavallo, L.; Chen, E. Y.-X. *J. Am. Chem. Soc.* **2012**, *134*, 7278−7281.
(37) Britovsek, G. J. P.; Gibson, V. C.; Wass, D. F. *Angew. Chem., Int. Ed.* **1999**, *38*, 428−447.
(38) Gibson, V. C.; Spitzmesser, S. K. *Chem. Rev.* **2003**, *103*, 283−315.
(39) Coates, G. W. *J. Chem. Soc., Dalton Trans.* **2002**, 467−475.
(40) Coates, G. W.; Hustad, P. D.; Reinartz, S. *Angew. Chem., Int. Ed.* **2002**, *41*, 2236−2257.
(41) Lamberti, M.; Mazzeo, M.; Pappalardo, D.; Pellecchia, C. *Coord. Chem. Rev.* **2009**, *253*, 2082−2097.
(42) Delferro, M.; Marks, T. J. *Chem. Rev.* **2011**, *111*, 2450−2485.
(43) Kawai, K.; Fujita, T. *Top. Organomet. Chem.* **2009**, *26*, 3−46.
(44) Jeon, Y-.M.; Park, S. J.; Heo, J.; Kim, K. *Organometallics* **1998**, *17*, 3161−3163.
(45) Tshuva, E. Y.; Goldberg, I.; Kol, M.; Goldschmidt, Z. *Chem. Commun.* **2001**, 2120−2121.
(46) Meppelder, G.-J. M.; Fan, H.-T.; Spaniol, T. P.; Okuda, J. *Organometallics* **2009**, *28*, 5159−5165.
(47) Ziniuk, Z.; Goldberg, I.; Kol, M. *Inorg. Chem. Commun.* **1999**, *2*, 549−551.
(48) van der Linden, A.; Schaverien, C. J.; Meijboom, N.; Ganter, C.; Orpen, A. G. *J. Am. Chem. Soc.* **1995**, *117*, 3008−3021.
(49) Baumann, R.; Davis, W. M.; Schrock, R. R. *J. Am. Chem. Soc.* **1997**, *119*, 3830−3831.
(50) Tshuva, E. Y.; Goldberg, I.; Kol, M. *J. Am. Chem. Soc.* **2000**, *122*, 10706−10707.
(51) Tshuva, E. Y.; Groysman, S.; Goldberg, I.; Kol, M.; Goldschmidt, Z. *Organometallics* **2002**, *21*, 662−670.
(52) Tshuva, E. Y.; Goldberg, I.; Kol, M. *Organometallics* **2001**, *20*, 3017−3028.
(53) (a) Groysman, S.; Goldberg, I.; Kol, M.; Genizi, E.; Goldschmidt, Z. *Inorg. Chim. Acta* **2003**, *345*, 137−144. (b) Groysman, S.; Goldberg, I.; Kol, M.; Genizi, E.; Goldschmidt, Z. *Organometallics* **2003**, *22*, 3013−3015.
(54) Segal, S.; Goldberg, I.; Kol, M. *Organometallics* **2005**, *24*, 200−202.
(55) (a) Yeori, A.; Goldberg, I.; Shuster, M.; Kol, M. *J. Am. Chem. Soc.* **2006**, *128*, 13062−13063. (b) Yeori, A.; Goldberg, I.; Kol, M. *Macromolecules* **2007**, *40*, 8521−8523. (c) Cohen, A.; Yeori, A.; Kopilov, J.; Goldberg, I.; Kol, M. *Chem. Commun.* **2008**, 2149−2151.
(56) Gendler, S.; Zelikoff, A. L.; Kopilov, J.; Goldberg, I.; Kol, M. *J. Am. Chem. Soc.* **2008**, *130*, 2144−2145.
(57) Cohen, A.; Kopilov, J.; Goldberg, I.; Kol, M. *Organometallics* **2009**, *28*, 1391−1405.
(58) Segal, S.; Yeori, A.; Shuster, M.; Rosenberg, Y.; Kol, M. *Macromolecules* **2008**, *41*, 1612−1617.
(59) Press, K.; Cohen, A.; Goldberg, I.; Venditto, V.; Mazzeo, M.; Kol, M. *Angew. Chem., Int. Ed.* **2011**, *50*, 3529−3532.
(60) (a) Kiesewetter, E. T.; Randoll, S.; Radlauer, M.; Waymouth, R. M. *J. Am. Chem. Soc.* **2010**, *132*, 5566−5567. (b) Randoll, S.; Kiesewetter, E. T.; Waymouth, R. M. *J. Polym. Sci., Part A: Polym. Chem.* **2012**, *50*, 2604−2611.
(61) Gowda, R. R.; Chen, E. Y.-X. *Dalton Trans.* **2013**, *42*, 9263−9273.
(62) (a) Zucchini, U.; Albizzati, E.; Giannini, U. *J. Organomet. Chem.* **1971**, *26*, 357−372. (b) Thiele, K.-H.; Köhler, E.; Adler, B. *J. Organomet. Chem.* **1973**, *50*, 153−159. (c) Giannini, U.; Zucchini, U.; Albizzati, E. *J. Polym. Sci., Part B: Polym. Lett.* **1970**, *8*, 405−410.
(63) Kol, M.; Shamis, M.; Goldberg, I.; Goldschmidt, Z.; Alfi, S.; Hayut-Salant, E. *Inorg. Chem. Commun.* **2001**, *4*, 177−179.
(64) Bryliakov, K. P.; Talsi, E. P. *Eur. J. Org. Chem.* **2008**, 3369−3376.
(65) Cameron, P. A.; Gibson, V. C.; Redshaw, C.; Segal, J. A.; Solan, G. A.; White, A. J. P.; Williams, D. J. *J. Chem. Soc., Dalton Trans.* **2001**, 1472−1476.
(66) (a) Sheldrick, G. *SADABS*; Bruker AXS, Madison, WI, 1997. (b) Sheldrick, G. *SHELXTL, version 6.14*; Bruker AXS, Madison, WI, 2004. (c) Spek, A. L. *J. Appl. Crystallogr.* **2003**, *36*, 7−13.
(67) (a) Bolig, A. D.; Chen, E. Y.-X. *J. Am. Chem. Soc.* **2004**, *126*, 4897−4906. (b) Rodriguez-Delgado, A.; Chen, E. Y.-X. *Macromolecules* **2005**, *38*, 2587−2594. (c) Zhang, Y.; Ning, Y.; Caporaso, L.; Cavallo, L.; Chen, E. Y.-X. *J. Am. Chem. Soc.* **2010**, *132*, 2695−2709. (d) Mariott, W. R.; Chen, E. Y.-X. *Macromolecules* **2005**, *38*, 6822−6832.
(68) (a) Chen, X.; Caporaso, L.; Cavallo, L.; Chen, E. Y.-X. *J. Am. Chem. Soc.* **2012**, *134*, 7278−7281. (b) Caporaso, L.; Cavallo, L. *Macromolecules* **2008**, *41*, 3439−3445. (c) Caporaso, L.; Gracia-Budrìa, J.; Cavallo, L. *J. Am. Chem. Soc.* **2006**, *128*, 16649−16654.
(69) Becke, A. D. *Phys. Rev. A* **1988**, *38*, 3098−3100.
(70) (a) Perdew, J. P. *Phys. Rev. B* **1986**, *33*, 8822−8824. (b) Perdew, J. P. *Phys. Rev. B* **1986**, *34*, 7406−7406.
(71) Weigend, F.; Ahlrichs, R. *Phys. Chem. Chem. Phys.* **2005**, *7*, 3297−3305.
(72) (a) Leininger, T.; Nicklass, A.; Stoll, H.; Dolg, M.; Schwerdtfeger, P. *J. Chem. Phys.* **1996**, *105*, 1052−1059. (b) Kuechle, W.; Dolg, M.; Stoll, H.; Preuss, H. *J. Chem. Phys.* **1994**, *100*, 7535−7542. (c) Haeusermann, U.; Dolg, M.; Stoll, H.; Preuss, H. *Mol. Phys.* **1993**, *78*, 1211−1224.
(73) (a) Tomasi, J.; Mennucci, B.; Cammi, R. *Chem. Rev.* **2005**, *105*, 2999−3093. (b) Barone, B.; Cossi, M. *J. Phys. Chem. A* **1998**, *102*, 1995−2001.
(74) For selected examples, see: (a) Sauer, A.; Kapelski, A.; Fliedel, C.; Dagorne, S.; Kol, M.; Okuda, J. *Dalton Trans.* **2013**, *42*, 9007−9023. (b) Licini, G.; Mba, M.; Zonta, C. *Dalton Trans.* **2009**, 5265−5277. (c) Chmura, A. J.; Davidson, M. G.; Frankis, C. J.; Jones, M. D.; Lunn, M. D. *Chem. Commun.* **2008**, 1293−1295. (d) Gendler, S.; Segal, S.; Goldberg, I.; Goldschmidt, Z.; Kol, M. *Inorg. Chem.* **2006**, *45*, 4783−4790. (e) Kim, Y.; Verkade, J. G. *Organometallics* **2002**, *21*, 2395−2399.
(75) (a) Chen, Y.-X.; Fu, P.; Stern, C. L.; Marks, T. J. *Organometallics* **1997**, *16*, 5958−5963. (b) Chen, Y.-X.; Marks, T. J. *Organometallics* **1997**, *16*, 3649−3657. (c) Bochmann, M.; Lancaster, S. J.; Hursthouse, M. B.; Malik, K. M. A. *Organometallics* **1994**, *13*, 2235−2243.

(d) Bochmann, M.; Lancaster, S. J. *Organometallics* **1993**, *12*, 633−640. (e) Jordan, R. F.; LaPointe, R. E.; Baenziger, N. C.; Hinch, G. D. *Organometallics* **1990**, *9*, 1539−1545.
(76) (a) Liang, L.-C.; Schrock, R. R.; Davis, W. M. *Organometallics* **2000**, *19*, 2526−2531. (b) Schrock, R. R.; Baumann, R.; Reid, S. M.; Goodman, J. T.; Stumpf, R.; Davis, W. M. *Organometallics* **1999**, *18*, 3649−3670. (c) Baumann, R.; Stumpf, R.; Davis, W. M.; Liang, L.-C.; Schrock, R. R. *J. Am. Chem. Soc.* **1999**, *121*, 7822−7836.
(77) (a) Klosin, J.; Roof, G. R.; Chen, E. Y.-X.; Abboud, K. A. *Organometallics* **2000**, *19*, 4684−4686. (b) Horton, A. D.; de With, J.; van der Linder, A. J.; van de Weg, H. *Organometallics* **1996**, *15*, 2672−2674.
(78) (a) Thorn, M. G.; Etheridge, Z. C.; Fanwick, P. E.; Rothwell, I. P. *J. Organomet. Chem.* **1999**, *591*, 148−162. (b) Chen, E. Y.-X.; Marks, T. J. *Chem. Rev.* **2000**, *100*, 1391−1434. (c) Scollard, J. D.; McConville, D. H.; Rettig, S. J. *Organometallics* **1997**, *16*, 1810−1812. (d) Phomphrai, K.; Fenwick, A. E.; Sharma, S.; Fanwick, P. E.; Caruthers, J. M.; Delgass, W. N.; Abu-Omar, M. M.; Rothwell, I. P. *Organometallics* **2006**, *25*, 214−220.
(79) Calculations indicated that decomposition of tetrabenzylzirconium to dibenzylzirconium plus two benzyl radicals is unfavored by a ΔG value of roughly 25−30 kcal/mol, relative to decomposition to tribenzylzirconium plus benzyl radical. This is in qualitative agreement with the experimental results reported in ref 62b.
(80) It is worth noting that the competitive toluene elimination reaction shows an energetic barrier at least 10 kcal/mol higher than that for the H transfer reaction, as shown in Scheme 5 (compare **TS′_1C** and **TS_1C** with **TS′_2B**).